SLAC P-399

POSITIVE PION PHOTOPRODUCTION FROM HYDROGEN
FOR INCIDENT PHOTON ENERGIES 300-750 MeV

C. Bétourné, J.C. Bizot
J. Perez-Y-Jorba, D. Treille

and

W. Schmidt

Stanford Linear Accelerator Center
Stanford University, Stanford, California, U.S.A.

L.A.L. 1186
February 1968

SLAC PUB 399
L.A.L. 1186
FEBRUARY 1968

POSITIVE PION PHOTOPRODUCTION FROM HYDROGEN FOR INCIDENT PHOTON ENERGIES 300-750 MeV

C. BETOURNE, J.C. BIZOT
J. PEREZ-Y-JORBA, D. TREILLE

Ecole Normale Supérieure
Laboratoire de l'Accélérateur Linéaire
91 - Orsay, France

W. SCHMIDT*

Stanford Linear Accelerator Center
Stanford University, Stanford, California, U.S.A.

ABSTRACT

The differential cross-section for the reaction $\gamma + p \rightarrow \pi^+ + n$ was measured at 19 photon energies, between 300 and 750 MeV in the laboratory, for pion angles between 0° and 130° in the center of mass system. The pions were analysed in angle and momentum with a magnetic spectrometer and detected by a counter telescope. The 0° measurements could be achieved, in spite of the excessive positron rate, owing to a mass spectrometer arrangement. No direct indication for the electromagnetic excitation of the P_{11}-resonance (1466 MeV) was found. Comparison is made with theoretical calculations of π^+ photoproduction.

* On leave of absence from Institüt für Experimentelle Kernphysik, Kernforschungszentrum, Karlsruhe, Germany.

I. INTRODUCTION

Many angular distributions of single π^+ photoproduction on protons are now available, up to a photon energy $k = 1270$ MeV.[1,2] In spite of the many data it was not possible to extend phenomenological analyses[3,4] in the region of the D_{13}-pion nucleon resonance ($k_R \approx 770$ MeV) to lower energies $k < 550$ MeV since the information was too scanty. But such an extension of the analyses is necessary in order to see if the results are consistent with the results of the dispersion theory at lower energies around the P_{33}-resonance. Such a check could remove at least part of the arbitrariness in formulating a phenomenological model at these higher energies.

The results, which we present in this paper for laboratory photon energies $k = 300 \ldots 750$ MeV serve mainly three purposes:

First, the new data supply small angle cross sections which are lacking between the highest measurement of Knapp et al.[5] and the lowest measurement of Beneventano et al.[6] ($k = 550$ MeV). These cross sections give a sensitive test for theoretical predictions near zero degree, where the results of the different theories usually do not agree.

Second, the results allow us to systematically study the effects of the P_{11}-resonance (1466 MeV) between the P_{33}(1236 MeV) and D_{13}(1525 MeV) resonances, where the data were rather scanty up to now.[7,8,9,10]

Third, we undertook to provide data with a better accuracy, in order to solve the question of discrepancies between various experimental results and to allow for a refinement of phenomenological predictions.

II. GENERAL FEATURES OF THE EXPERIMENTAL METHOD

π^+ are photoproduced by sending a bremsstrahlung beam on a liquid hydrogen target. They are analysed by a magnetic spectrometer at momentum p and laboratory angle θ.

The kinematics of the reaction is described by Fig. 1, where k is the laboratory energy of the photon. The energy E of the machine is chosen so that k belongs to the flat region of the bremsstrahlung energy curve; but E is below threshold for double photoproduction processes giving a π^+ at the analysed momentum.† Tests of consistency of our energy calibrations were obtained by drawing excitation curves at fixed p and θ and variable E (Fig. 2).

In addition to π^+ other particles are analysed and reach the detectors. These are essentially protons from π° photoproduction and, at forward angles, positrons from electromagnetic pairs. We have, on Fig. 1, distinguished three regions that we define now. E^+, P, Π^+ represent the yield of analysed e^+, p, π^+.

<u>region 1</u>	<u>region 2</u>	<u>region 3</u>
$P > \Pi^+$	$P > \Pi^+$	$P \lesssim \Pi^+$
$E^+ > \Pi^+$	$E^+ < \Pi^+$	$E^+ \sim 0.01\ \Pi^+$

In region 3 the small constant rate of e^+ comes from π° decay. In region 1, the rate of e^+ increases very rapidly at small angles, and at 0°, even in the most favorable experimental conditions, the ratio E^+/Π^+ is as high as $\sim 10^4 - 10^5$. Besides e^+ and p, some muons from π^+ decay reach also the detection system.

The two leading factors governing possibilities of discrimination at detection are the following:

†In fact E was kept below threshold for $\mu^+\mu^-$ production giving a μ^+ at the analysed momentum.

a. Because of the linear accelerator poor duty cycle (5.10^{-5}) one must limitate total counting rates ($<$ 30-40 counts per second) to avoid large and poorly known dead time losses in the electronics. This sets a lower limit to the time needed for registering a given number of π^+ and the presence of additional background increases this limit.

b. The limited possibilities of discrimination of the detection system, which will be described later, obviously lead to a possibility of confusion between particles when the rate of background particles is high.

A very conservative rule was applied: when, after analysis, the ratio of the number of background particles over Π^+ is equal to or larger than one, one eliminates (totally or partially) the spurious particles in an appropriate way before detection. So, in region 1, both e^+ and protons are eliminated; in region 2, only protons. The case of μ^+, that we could neither eliminate nor discriminate in the whole range of our measurements, has been treated by computation, the result of the computations being checked by a separate experiment. As a consequence the experimental procedure is different in each region as seen later. The overlap of two different procedures, near the border of two domains, provides very useful tests of reliability.

The elimination of background before detection is a source of π^+ loss through strong interactions and multiple scattering. So, except in region 3, one does not obtain at once the real number of analysed π. But the π loss, for a given experimental setup and especially for a given analysed momentum p, is independent of the angle θ. Therefore, everything being left unchanged except θ (and E), one goes from the measurement point M (or M') (Fig. 1) to some "normalization" point N belonging to region 3. From the ratio of π rates in M (or M') and N, the π loss disappears. Now, this ratio is, up to kinematical factors, equal to the ratio of the corresponding photoproduction cross sections and since the absolute cross section can be determined in N, we thus get the absolute one in M. So one can say that the measurement is direct in region 3, indirect in regions 1 and 2: anyway in both cases one reaches absolute cross sections.

III. EXPERIMENTAL ARRANGEMENT

- The electron beam is extracted from the linear accelerator by an achromatic afocal system composed of three magnets (Fig. 3). A slit before magnet 2 reduces the beam energy resolution to the desired value ($\Delta E/E = 2\%$ in our case). The average energy E is measured with a proton resonance probe. Two quadrupoles Q_1, Q_2 allow for the focalisation of the beam on the target . A secondary electron emission monitor, of thickness 2.10^{-4} radiation length and stability better than 0.5%, is used to measure the intensity of the electron beam: it can be calibrated against a Faraday cup which is removed from the beam during data taking to reduce background.

- The photon beam is produced in a radiator after which the charged particles are swept by a magnet; the radiator thickness is computed to avoid any further collimation of the bremsstrahlung beam. Foils of copper or aluminium from .5% to 4% radiation length were used as radiators. The photon spectrum was computed with a thick target bremsstrahlung program[11] which takes into account the electron energy degradation in the radiator and pair production by the photons.

- The liquid hydrogen is contained in an appendix (Fig.4) (55 x 210 mm, 60 mm height) with 50 μ steel windows, which is directly connected to a ten liters liquid hydrogen reservoir, both being enclosed in a vacuum chamber.

- In region 3 this vacuum chamber is connected to the spectrometer and can rotate with it (Fig. 4a). The target major axis and the spectrometer optical axis coincide. A tungsten collimator set parallel to this axis with a good accuracy prevents the spectrometer from seeing the target windows and thus eliminates the empty target background as it has been checked. It also reduces to 35 mm the transverse target width as seen by the spectrometer; so the useful interaction length of the beam is $35/\sin\theta$ (mm). The electron energy E was always chosen to avoid any contamination from energetic π^+ produced at the end of the bremsstrahlung spectrum and losing energy in the collimator.

In regions 1 and 2 the target vacuum chamber is independent of the spectrometer. The target is roughly normal to the beam (Fig.4b) and the empty target background has to be subtracted. In these regions because of the normalization process used one need not know the exact target length, as it will appear later.

The magnetic spectrometer[12] (Fig.5) is made of three magnets which are electrically set in series. The whole system is symmetric relative to the bissector plane R of magnet 2.

In first order optics, this spectrometer is triple focusing and its magnification is one.

In the radial plane:

α. There exists in plane R an intermediate image: all trajectories of same momentum p_o and coming from a point O are focused there in a point C, whatever be their emission angle in the radial plane.

β. The radial abscissa in plane R for a trajectory of momentum p depends on the relative difference $\frac{p-p_o}{p_o}$ between p and the central momentum p_o. So one can determine the momentum resolution $\Delta p/p_o$ by a radial slit in plane R. $\Delta p/p_o$ was $\pm 2\%$ in this experiment.

In the transverse plane:

α. The trajectories are independent of momentum.

β. The transverse abscissa in plane R depends only on the transverse angle at emission.

γ. A suitable transverse slit in plane R can be used to make the solid angle constant for all points of the target, whatever be their distance to the spectrometer optical axis.

These optical properties, especially the existence of a radial intermediate image in plane R, allow for another use of this apparatus, in a mass spectrometer way, as we shall see later.

The spectrometer calibration was performed with the floating wire technique and its accuracy is 0.5%. The maximum momentum one can reach is limited to 600 MeV/c by magnet saturation.

In regions 2 and 3 the solid angle was defined by the spectrometer optics itself and not by some entrance slits. It was measured at several momenta through an experiment of e^-p elastic scattering, as will be seen later. The angular resolution was $\pm.8°$ lab. in the transverse plane and $\pm5°$ lab. in the radial one, except for the measurements of region 1 where this last value was lowered to $\pm2°$ lab.

IV. PARTICLE SEPARATION AND IDENTIFICATION OF PIONS

As we explained previously the structure of the detection system depends on the region explored:

Region 3: The telescope is made of three plastic scintillators designed so as to collect all particles analysed by the spectrometer. On each counter a bias separates low signals due to the majority of the π^+ from high signals due to the protons and to about 10% of the π^+ belonging to the tail of the ionization loss spectrum. Proton signals are high in all three counters, while there is no correlation between the value of a π signal from one scintillator to another. Therefore such a bias allow to eliminate all protons without losing more than one π out of one thousand.

On the other hand this telescope does not permit to separate the muons from the π mesons. This μ contamination must be computed and the calculation will be described in part V.

Region 2: Protons being here more numerous than pions, are stopped before detection in a carbon absorber set just in front of the telescope. The π loss in the absorber is taken into account as described before, in going from point M to point N: it can reach 60%, when the π momentum corresponds to the first resonance πN. A gas Cerenkov detector rejects the positrons; the pions are detected as before with three plastic scintillators.

Region 1: The rate of the positrons is very important. One cannot eliminate them by means of an absorber in front of the counters. Indeed it is well known that positrons in matter develop showers and, even after several radiation lengths, e^+ and e^- of small energy are still present.

On the other hand pions lose only a small fraction of their momentum by ionization. Such a difference of behavior suggests the possibility of a magnetic separation between the pions and the showers components, the quasi totality of which has momenta much smaller than the pions momenta.

This separation was achieved with the previously described spectrometer used in a different way (Fig.6). It was magnetically separated in two parts, the first two magnets on one side, the third one on the other, a lead radiator of 1 to 6 radiation lengths was set near plane R.

The first part analyses the particles according to their momentum around p_o. In the radiator they undergo the previously described processes. Then, the second part analyses the particles according to their loss of momentum in the radiator as seen below. If the second part is set to the average momentum p_π of the π^+ coming out from the absorber, the mesons thus reach the counters, while the quasi totality of the showers components are swept.

Because of the existence of an intermediate image in plane R, the total spectrometer is still focusing in energy and in radial angle, in spite of multiple scattering in the radiator, but only for particles losing the same momentum δp in this radiator. Correspondingly, a difference of momentum loss in the radiator is changed into spatial dispersion in the image plane.

So one must now distinguish two resolutions:

- A resolution in analysed momentum $\Delta p/p_o$, determined as previously by radial slits.

- A resolution in momentum loss δp in the radiator determined by the radial size of the counters in image plane.

These two functions of the spectrometer are completely independent.

In the transverse plane, the spectrometer is no more focusing because of multiple scattering and the resulting loss of π can reach 90%. The previously described normalization procedure accounts perfectly for this loss. One may notice that the loss of π through strong interactions in the lead radiator is less than 20%. The effect of a transverse slit is the same as before.

Fig. 7 shows the e^+ and π^+ spectra as a function of momentum in the third magnet: the ratio E^+/Π^+ at the pion peak still goes from 0.5 to 10 at 0°. So one needs a subsequent discrimination at detection.

It was achieved by a gas Cerenkov counter working with freon 13 under 12 bars, of efficiency .997 $\pm$ .003 to e^+. The uncertainty (.003) on this efficiency makes 0° measurements below 300 MeV imprecise because the ratio E^+/Π^+ increases very rapidly there.

Electronics: Discriminators and coincidence units are standard Chronetics circuits running on 50 MHz ($\sim$ 15 ns coincidence resolution). The countings are recorded on 100 MHz scalers, which can register up to four events within the accelerator pulse ($\sim$ 1 μs).

V. DATA REDUCTION

One will consider separately the direct measurements of region 3 and the indirect ones of regions 1 and 2. To determine the absolute cross section one must know the detection solid angle and apply several corrections. On the other hand the indirect measurements essentially give a ratio between two cross sections: the corrections can be ignored if they are the same at measurement and normalization points. This is almost correct since they depend mostly on the π momentum which is identical at both points. In the same way, the solid angle completely disappears from the ratio.

a. Absolute Measurements

1. Solid angle determination. The solid angle was determined by measuring, with the same experimental setup, e^-p elastic scattering at several momenta of the final electrons and for low transfers, where the proton form factors are known with great accuracy; the photoproduction spectrum is rather flat on the spectrometer momentum acceptance (curve a of Fig. 8) while an elastic peak intrinsic width (curve b) is much smaller than this 4% acceptance. Thus to take into account the variation of solid angle with momentum inside this acceptance (curve c) we folded the elastic peak distribution curve with the momentum acceptance by moving the spectrometer central energy q around the fixed energy p_o of the maximum of the elastic peak. We then obtained curve d by dividing the folding by the acceptance (.04 q). From the area S under curve d we get the solid angle of the apparatus integrated over the target length L and the spectrometer momentum acceptance $A = \frac{\Delta p}{p_o}$ around momentum p_o:

$$\overline{\Omega} = \frac{1}{AL} \iint \Omega \, dA \, dL \tag{1}$$

through the relation:

$$S = \frac{d\sigma_R}{d\Omega} \, C(\Delta) \, \overline{\Omega} \, F \tag{2}$$

Here F is the product of the number of incident electrons by the density of target protons per cm^2. $\frac{d\sigma_R}{d\Omega}$ is the Rosenbluth cross section. $C(\Delta)$ is a correction factor due to the fact that the tail of curve d is truncated at $p_o - \Delta$. A good approximation to $C(\Delta)$, if Δ is sufficiently large (fairly larger than the half width of curve d), is to take the usual form for a normal non folded elastic peak.(13) But this correction is valid only for $\Delta/p_o \ll 1$, while, as we said, we deal with rather high values of Δ. Therefore, we performed slight modifications to $C(\Delta)$ to take into account the fact that, when Δ is large, scattering after radiation and scattering before radiation, leading to the same final energy, occur in fact at different energies. Thus one found that for a given momentum, the value obtained for $\overline{\Omega}$ was constant within 1% when Δ/p_o was varied from 3 to 15%.

Figure 9 shows the variation of $\overline{\Omega}$ as a function of momentum. The error on $\overline{\Omega}$ is estimated to 2.5%.

2. Corrections. Along the distance from the target to the counters (10 m), an important fraction of the pions, which can reach 60%, decays with emission of a muon in a very small forward cone.

The counting rate is corrected for the π exponential decrease and for μ^+ contamination, the μ^+ being indistinguishable from π^+ at detection. The formulation of the μ contamination problem was treated through a Monte-Carlo method with the following random variables:

- the π momentum and direction at emission,
- its length of flight, according to an exponential law,
- the μ emission angles (determining its momentum).

The trajectories in the spectrometer were computed to first order. The calculated μ^+ contamination varies from 12% to 6% of the number of detected π^+ and is thought to be accurate to 2% of this number.

These computations were checked at low momentum by detecting selectively muons with a water Cerenkov counter. The agreement is satisfactory.

Before leaving the target, pions traverse ten cm of hydrogen. Because of the very small angular acceptance of the spectrometer, a pion which undergoes a strong interaction is lost: this effect can reach 10% on the first πN resonance. On the other hand, some π, which initially do not satisfy requirements to be analysed, may scatter on a proton and subsequently fulfil these requirements: this correction never exceeds 2%.

Electromagnetic effects in the target are twofold:

- Positive and negative contributions due to multiple scattering cancel one another.

- The momentum loss by ionization, especially at low energies, changes with momentum inside the accepted band: therefore there may be a 3% difference between the acceptance as being determined by radial slits and its effective value when π are produced. This effect has been accounted for.

In the telescope, similar phenomena occur, the results of which is a decrease of the counting efficiency. By strong interactions in the two first counters, pions are lost: this loss, being a linear function of the thickness of these two counters, has been measured by varying artificially their thickness using additional absorbers of the same material. Multiple scattering has a very small effect, and was neglected.

The counting rates have been corrected for accidental coincidences and electronic losses which are mainly due to the discriminators dead times.

3. Cross section computation. Once the correct pion rate N_π has been obtained, the cross section in the laboratory system is extracted from the formula:

$$N_\pi = N_\gamma \, n_P \, \frac{d\sigma}{d\Omega}(k,\theta) \, \bar{\Omega}(p_o) \tag{3}$$

where the photon number N_γ is given by

$$N_\gamma = N_e \, \rho(k) \, \Delta k \tag{4}$$

N_e = electron number

$\rho(k)$ = bremsstrahlung spectrum density per electron

Δk = photon energy resolution = $\frac{\partial k}{\partial p}(p_o,\theta)\Delta p$

n_P = proton density per cm^2 along the beam direction.

The photon energy resolution Δk is large at high energies and backward angles: therefore the cross sections have been corrected in consequence.

b. Indirect Measurements

In regions 1 and 2, where the target is transverse, we need an empty target subtraction which can reach 20% at 0° and low energies.

As said before, the small angle cross section is obtained from a normalization procedure at an angle α and same momentum p, where the absolute cross section is known by direct measurement; the ratio of cross sections and the ratio of counting rates at $\theta°$ and $\alpha°$ are simply related by:

$$\frac{N_\pi(\theta)}{N_\pi(\alpha)} = \frac{\frac{d\sigma}{d\Omega}(k(\theta),\theta)\; N_\gamma(\theta)}{\frac{d\sigma}{d\Omega}(k(\alpha),\alpha)\; N_\gamma(\alpha)} \tag{5}$$

For each measurement at small angles we have chosen at least two normalization points corresponding to two different angles α: the cross sections at these angles α were computed by interpolation between the absolute results of region 3. As expected we obtained the same value for the small angles cross sections, within statistics, whatever be α.

In going from θ to α the effective target length L seen by the spectrometer changes as shown in Fig. 4b. But as already noted, a transverse slit in the symmetry plane of the spectrometer has been designed to make the acceptance constant for all points of interaction in the target, up to the largest angle α used for normalization. This has been checked experimentally. Therefore the parameter L has no influence on the counting rates. We have also checked that the choice of the resolution in loss of momentum δp does not modify our results.

In the determination of the cross sections ratio all the previously described corrections (π decay, μ correction, π losses, etc.) cancel to first order and only their small differences between θ and α have to be accounted for.

VI. RESULTS

Table I gives the differential cross sections in the center of mass system, as a function of the pion center of mass angle θ^* for 19 values of the laboratory photon energy. The result quoted is often the weighted mean of several measurements. The random errors listed represent the statistical error added quadratically to the errors on the dead time correction and on the secondary electron monitor efficiency. For the indirect measurements, it also includes the normalization uncertainty ($\sim$ 3%). Below 600 MeV, the total cross sections were obtained from least square fits of our data, the weight of the backward angles which are missing in our data being negligible. Above 600 MeV, Moravcsik fits were used for the forward angles which are lacking in our data, the contribution of these points being also very weak.

The pion angle θ is known to about 3'. The corresponding resolution is $\Delta\theta = .8°$ lab.; the azimuthal resolution $\Delta\phi = \pm 5°/\sin\theta$ lab. does not affect the results in regions 2 and 3; in region 1 the angular resolution was always smaller than $\pm 2°$ lab. and the quoted results have not been unfolded from this resolution. Fit of the data with a Moravcsik curve shows a negligible influence of this resolution. It is then thought that this effect is appreciably smaller than the other experimental errors.

The photon energy calibration is consistent from point to point to about .1% and the absolute calibration error is less than .5%. The energy resolution depends on the pion momentum and angle and is essentially defined by the spectrometer momentum resolution (4%).

The systematic errors are listed in Table II. The cross sections are plotted on Fig. 10 and 11 to allow for a direct comparison with previous data.[1,2,6-9,14-20] The figure 12 shows excitation curves for fixed values of θ^*.

VII. DISCUSSION OF THE RESULTS

Below $k = 500$ MeV the new results of this experiment can be compared to absolute predictions following from a new evaluation of fixed-t dispersion relations.[21,24] Above $k = 500$ MeV only phenomenological approaches exist so far.[3,4] The work in Ref. (3) is an extension of the dispersion model at low energies,[21] and we shall mainly base our discussion on those results.

a. General Review

It has been discussed in Ref. (22) that at present our incomplete knowledge of high energy contributions in dispersion integrals leaves arbitrary certain contributions to the multipoles $M_{1+}^{3/2}$ and $E_{1+}^{3/2}$ (23) of the first resonance, which vary slowly with energy. As a consequence one is only able to predict the large $M_{1+}^{3/2}$ at resonance within 5 ... 10% and one cannot predict the sign of the small quantity $E_{1+}^{3/2}$ from theory alone. But once $M_{1+}^{3/2}$ $(k = k_R)$ and $E_{1+}^{3/2}$ $(k = k_R)$ are fixed, the energy dependence within the region of the first resonance can safely be predicted for these partial amplitudes. Therefore an effort was made in Ref. (21) to narrow the limits for the parameters $M_{1+}^{3/2}(k_R)$ and $E_{1+}^{3/2}(k_R)$ by fitting certain experimental quantities, which depend sensitively on these parameters. In this way the uncertainty with respect to $E_{1+}^{3/2}(k_R)$ could be reduced considerably and the limits for $M_{1+}^{3/2}(k_R)$ could be made smaller than 5%. The experimental results used were mainly obtained with plane-polarized γ's in π°-photoproduction. Therefore the dispersion theory results for π^+-photoproduction presented here in Figs. 10, 11, 12 are a prediction (the results correspond to the best solution in Ref. (21)).

One observes in Figs. 10, 11, 12 reasonably good agreement. Around the first resonance the largest discrepancies appear near $\theta^* = 90°$, where the theory predicts differential cross sections which are too large. If the parameters chosen to fix $M_{1+}^{3/2}$ and $E_{1+}^{3/2}$ are correct, then one would clearly see here the influence of errors in the small multipoles which should be enhanced around the resonance. But the differences between theory and experiment are never larger than has to be expected (see e.g. the errors on the theoretical predictions calculated in Ref. (24)).

The reasonably good agreement of the dispersion theory results extends to rather high energies (k = 500 MeV). Therefore one can expect that the direct extension of the dispersion isobar model into the region of the second resonance ($k \approx 750$ MeV) should yield a reasonable approximation for the background amplitude; i.e. one should expect changes only in a few physically relevant partial amplitudes, e.g. in those cases where new resonances occur. A phenomenological fit to the data along these lines has been given in Ref. (3). Some results above k = 500 MeV are shown in Fig. 10 and 12. The main changes with respect to the first isobar background amplitude appear in the multipoles E_{2-}, M_{2-} of the D_{13}-resonance and in the S-wave E_{0+}. There is at the moment a theoretical gap around k = 550 MeV because of the lack of data at the time the analysis in Ref. (3) was carried out.

b. The Near Forward Direction

Near the forward direction the dispersion theory results yield particularly good agreement around the first resonance. According to the results in Ref. (3) the discrepancies, which show up at higher energies near the forward direction, can be explained mainly by a small S-wave correction $\Delta \mathrm{Re} E_{0+}$, which could arise from unknown high energy contributions in dispersion integrals. The difference should not be due to the D_{13}-resonance because of the ratio

$$E_{2-}/M_{2-} \approx 3 \qquad (6)$$

for the contribution of this resonance.[3] With the ratio (6) the multipoles E_{2-} and M_{2-} cancel each other in forward and backward direction.

There is a marked discrepancy near the forward direction between the dispersion theory calculations in Ref. (21) and Ref. (24). According to Ref. (24) a narrow peak at approximately $\theta^* = 10°$ with a dip in forward direction should appear in the considered energy region. Such a behavior of the angular distributions can only occur by differences in very high partial amplitudes. The present data definitely exclude the possibility for such a dip. This is also more compatible with older calculations of Donnachie et al.[25]

According to the phenomenological approach in Ref. (4) the forward peak in the region of the second resonance is explained by the presence of the P_{11} (1466 MeV), S_{11} (1591 MeV), and S_{31} (1635 MeV) resonances. Therefore it is expected in Ref. (4) that at energies above these resonances the forward peak should drop sharply. But by the same argument one might then expect a drop of the forward peak below these resonances. The experimental data and the dispersion theory results presented here show clearly that the peak in forward direction is already present at lower energies ($k < 450$ MeV). Also at high energies the data of Ref. (1), (26) do not show the guessed sharp drop of the peak in forward direction. On the other hand in the approach of Ref. (3) the forward peak is predominantly an effect which arises by the interference of the pole-term with a dispersion integral contribution produced mainly by the first resonance. In this model no sharp drop of the peak is expected, since the higher resonances give only a small contribution in forward direction. It has been shown in Ref. (27) that with this model the forward peak can be explained up to very high energies $k > 1$ GeV. From the point of view of dispersion theory the forward peak in π^+-photoproduction presents no difficulty.

c. The P_{11}-Resonance (1466 MeV)

Particular care should be taken to look for an influence of the P_{11}-resonance on the data around $k = 670$ MeV. The resonance should affect the $J = 1/2$ multipole M_{1-}.

An elucidation of the electromagnetic properties of the P_{11}-resonance would supply criteria for its classification within symmetry schemes. Lovelace(28) suggested some time ago that the P_{11}-resonance should be a member of an anti-decuplet $\{\overline{10}\}$. In this case one has the very interesting consequence that the electromagnetic excitation of the P_{11}-resonance on the proton should be strongly suppressed by U-spin conservation.(29) As a member of the $\{\overline{10}\}$ representation, the P_{11}-resonance would belong to U-spin 1 and 3/2 multiplets. Therefore, the decay of P_{11} into (γ,n) with $U = 1$ is allowed but decay into (γ,p) with $U = 1/2$ is forbidden. In the conventional description this would be explained as follows: the isovector $M_{1-}^{1/2}$ and the isoscalar parts M_{1-}^{o}, which both lead into final states with isospin $I = 1/2$, appear in reactions on the proton and neutron with a different sign

$$(\gamma,p) \;:\; M_{1-}^{o} + \frac{1}{3} M_{1-}^{1/2} \tag{7a}$$

$$(\gamma,n) \;:\; M_{1-}^{o} - \frac{1}{3} M_{1-}^{1/2} \tag{7b}$$

Therefore, if

$$M_{1-}^{o} \approx \mp \frac{1}{3} M_{1-}^{1/2} \tag{8}$$

there will be an enhancement in the one case and a cancellation in the other. Relation (8) with the upper sign is generally true in the isobar approximation.(3,21) On the basis of the very scanty data on π^+, π^- -photoproduction it is expected(3) that relation (8) with the upper sign is satisfied by the contribution of the P_{11}-resonance. For a more detailed discussion see Ref. (3), (30).

Now, the π^+-excitation curves (Fig. 12) from the present data and the total cross section Fig. 11 indeed do not reveal any obvious structure around $k = 670$ MeV that could unambiguously indicate the excitation of this resonance on the proton. One observes only a smooth increase of the cross section in this energy region, which should be mostly due to the tail of the strong D_{13}-resonance. But from visual inspection of the systematic measurements in this energy region one can only conclude

a. that the excitation of the P_{11}-resonance in π^+-photoproduction is either weak, or

b. it is strong but cannot be detected visually because of its large width, low J-value and the high inelasticity. It could happen that this resonance can only be distinguished from the smooth background amplitude by using detailed models or partial-amplitude analyses.[3,4] In pion-nucleon scattering one is now very often confronted with such a situation.[31]

In π^+ and π° -photoproduction on the proton the same isospin combination of multipoles appears, which lead into the isospin $I = 1/2$, P_{11}-final state

$$M_{1-}^{\pi^+} = \sqrt{2}\,(M_{1-}^{o} + \frac{1}{3}\;M_{1-}^{1/2} - \frac{1}{3}\,M_{1-}^{3/2}) \tag{9a}$$

$$M_{1-}^{\pi^\circ} = M_{1-}^{o} + \frac{1}{3}\;M_{1-}^{1/2} + \frac{2}{3}\,M_{1-}^{3/2} \tag{9b}$$

Therefore in π°-photoproduction the situation with respect to the P_{11}-resonance should be similar.

Contrary to the phenomenological approach in Ref. (3) one has to conclude from the work in Ref. (4) that the electromagnetic excitation of the P_{11}-resonance on the proton is strong. In both works[3,4] a partial amplitude analysis was tried (in a restricted sense) by different methods; but the present data were not then available.

In Ref. (3) an approximate background amplitude, which is derived from the P_{33}-isobar approximation, is used as input. Thus it is possible to restrict from the very beginning the high ambiguity which one encounters in this kind of work. A fit to the data is then obtained by adjusting the physical relevant partial amplitudes individually. In Ref. (4) the fullest possible use of the known pion-nucleon scattering phase shifts is made by using an isobar model for the resonances and imposing the Watson theorem on the elastic partial amplitudes. The free parameters are then fitted to the available data. Especially in π°-photoproduction all details of the data are not fully understood as a result of insufficient experimental and theoretical information.

In all processes considered both methods yield completely different results for the $J = 1/2$ multipoles E_{0+} and M_{1-}. This may explain the different conclusion with respect to the role of the P_{11}-resonance. Of course, the results for the $J = 1/2$ multipoles are particularly ambiguous, since there the multipoles determine mainly the slowly varying background, which is usually not uniquely fixed because of systematic errors between different experimental groups.

However at present it seems very unlikely that unknown high energy contributions in the dispersion integrals for the $J = 1/2$ multipoles E_{0+} and M_{1-} can produce a rapid change with energy between $k = 500$ MeV and 600 MeV for both multipoles and thereby reconcile the results of Ref. (4) with the isobar approximation[21,24] at lower energies. Furthermore the energy variation of E_{0+} and M_{1-} is also restricted by the smooth behavior of the forward peak (see VII.b).

So it is at present more likely that the electromagnetic excitation of the P_{11}-resonance on the proton is forbidden, as suggested by naive visual analysis of the present data.

ACKNOWLEDGEMENTS

Our thanks go to Professor A. Blanc-Lapierre for extending to us the facilities of the Orsay Laboratory. We wish to thank Mr. Brochard and Mr. Richard for assistance in data taking, Messrs. Bouvard and Lissilour for help in the installation of the experiment. Two of us (C.B. and J. P-Y-J) are grateful to Dr. Nguyen Ngoc for assistance in the design and test of the Cerenkov counter. We are grateful for the help provided by the technological group directed by Mr. Round and by the accelerator team directed by Dr. Burnod and Dr. Milman.

Table I

Differential cross sections in the c.m. system (μb/sr)
and associated standard deviation errors Δ(μb/sr).
The π^+ c.m. angle is θ^*(degrees), the laboratory photon energy k (MeV).
The total cross section σ_T is in μb.

θ^*	σ	Δ
k = 300		
0.	8.1	1.4
2.7	8.2	.8
4.	8.4	.5
6.7	8.3	.5
10.	8.3	.5
13.3	8.3	.5
k = 310	σ_T = 223	
50	14.71	.41
60	16.78	.47
70	19.13	.54
80	21.08	.59
90	21.09	.59
100	20.77	.57
110	20.35	.57
120	20.33	.57
k = 325	σ_T = 212	
0.	14.2	.7
2.7	14.9	.8
50	15.93	.46
60	17.23	.50
70	18.33	.53
80	19.56	.57
90	19.62	.58
100	19.36	.58
110	18.88	.58
120	18.08	.56
k = 350	σ_T = 180	
0.	18.4	.8
2.	17.8	.9
2.7	18.4	.8
5.	18.7	1.3
7.5	16.7	1.2
10.	17.5	1.3
15.	14.9	1.0
50	15.07	.43
60	16.17	.46
70	16.20	.46
80	16.81	.48
90	16.62	.48
100	14.84	.44
110	14.48	.44
120	13.61	.41
130	13.37	.41
k = 375	σ_T = 141	
0.	20.0	.7
50	12.46	.34
60	13.77	.38
70	13.16	.37
80	12.82	.37
90	12.01	.35
100	11.44	.33
110	10.70	.31
120	10.03	.30
130	10.18	.31

Table I (cont.)

$k = 400 \qquad \sigma_T = 117$

θ^*	σ	Δ
0.	18.7	.9
2.5	19.5	.7
4.6	18.5	.7
7.	18.6	.7
10.	16.4	.8
14.5	15.5	.6
21.	13.4	.5
32.	12.9	.6
50	11.41	.31
60	11.33	.31
70	11.11	.31
80	10.37	.29
90	9.42	.27
100	8.62	.25
110	8.00	.23
120	7.12	.21
130	6.80	.23

$k = 425 \qquad \sigma_T = 97$

θ^*	σ	Δ
0.	20.6	.7
60	9.75	.26
70	9.04	.24
80	8.85	.24
90	7.95	.22
100	6.84	.19
110	6.43	.18
120	5.35	.16
130	5.55	.16

$k = 450 \qquad \sigma_T = 88$

θ^*	σ	Δ
0.	19.4	.8
2.9	18.4	.8
4.3	17.9	.7
7.2	16.8	.7
10.8	15.3	.6
13.5	14.2	.5
21.	11.1	.5
30	10.34	.27
40	9.42	.25
50	9.72	.25
60	9.14	.24
70	8.78	.23
80	7.91	.21
90	7.07	.19
100	6.25	.18
110	5.57	.16
120	4.55	.13
130	4.40	.13

$k = 475 \qquad \sigma_T = 85$

θ^*	σ	Δ
0.	18.8	.8
30	10.42	.27
40	9.64	.25
50	9.03	.23
60	8.77	.23
70	8.10	.21
80	7.54	.20
90	6.60	.18
100	5.79	.16
110	4.96	.14
120	4.17	.12
130	3.95	.11

Table I (cont.)

θ^*	σ	Δ
k = 500	σ_T = 81	
0.	18.3	.9
2.2	17.3	.6
5.	17.2	.7
7.3	15.8	.6
10.	14.1	.5
15.	12.3	.5
20.	10.7	.4
30	10.02	.31
40	9.57	.25
50	9.14	.24
60	8.15	.21
70	7.91	.20
80	7.23	.19
90	6.47	.17
100	5.38	.15
110	4.65	.13
120	4.04	.12
130	3.62	.10
k = 525	σ_T = 81	
0.	19.8	.9
30	10.62	.33
40	9.63	.30
50	9.26	.28
60	8.38	.22
70	7.96	.20
80	7.28	.19
90	6.50	.17
100	5.52	.15
110	4.58	.13
120	3.93	.11
130	3.46	.10

θ^*	σ	Δ
k = 550	σ_T = 80	
0.	18.9	.6
2.25	18.7	.6
5.0	18.0	.6
7.5	16.7	.5
10.6	15.0	.5
15.0	12.9	.4
21.2	10.7	.3
30	10.35	.32
40	9.80	.30
50	9.35	.28
60	8.63	.26
70	7.81	.20
80	7.16	.18
90	6.10	.16
100	5.27	.14
110	4.23	.11
120	3.54	.10
130	3.32	.10
k = 575	σ_T = 83.5	
0.	19.3	.9
5.3	18.0	.6
7.5	15.8	.5
10.	15.5	.5
15.	13.6	.5
20.	11.3	.4
30	10.84	.34
40	10.75	.33
50	10.19	.31
60	9.21	.28
70	7.93	.24
80	7.15	.18
90	6.45	.16
100	5.20	.14
110	4.46	.12
120	3.77	.10
130	3.45	.10

Table I (cont.)

θ^*	σ	Δ
$k = 600$	$\sigma_T = 83$	
0.	20.6	.9
2.3	21.	.9
5.	19.1	.6
7.6	17.5	.6
10.6	15.8	.6
15.1	14.2	.6
20	11.38	.35
30	10.13	.31
40	10.29	.32
50	10.28	.30
60	9.82	.29
70	8.23	.24
80	7.09	.18
90	6.21	.16
100	5.12	.13
110	4.41	.12
120	3.67	.10
130	3.26	.10
$k = 625$	$\sigma_T = 86$	
20	11.05	.34
30	10.59	.33
40	10.78	.33
50	10.42	.31
60	10.41	.31
70	9.01	.26
80	7.58	.22
90	6.22	.16
100	5.26	.13
110	4.54	.12
120	3.75	.10
130	3.40	.10
$k = 650$	$\sigma_T = 91$	
40	11.43	.35
50	11.15	.33
60	10.74	.32
70	9.78	.29
80	8.44	.25
90	6.76	.17
100	5.82	.15
110	4.66	.12
120	4.00	.11
130	3.61	.10
$k = 675$	$\sigma_T = 96$	
60	11.39	.32
70	9.97	.28
80	9.11	.26
90	7.66	.22
100	6.25	.16
110	5.29	.13
120	4.53	.12
130	3.92	.11
$k = 700$	$\sigma_T = 102$	
60	11.96	.34
70	10.65	.30
80	9.89	.28
90	8.35	.24
100	6.71	.17
110	6.02	.15
120	5.26	.14
130	4.66	.12

Table I (cont.)

θ^*	σ	Δ	θ^*	σ	Δ
$k = 725$	$\sigma_T = 96$		$k = 750$	$\sigma_T = 86$	
70	9.57	.27	70	8.35	.24
80	9.04	.26	80	7.70	.22
90	8.39	.24	90	7.59	.22
100	6.81	.20	100	6.30	.18
110	6.27	.16	110	5.60	.14
120	5.49	.14	120	5.00	.12
130	4.78	.13	130	4.48	.12

Table II

Systematic Errors

Source	Error
Bremsstrahlung spectrum	2 %
Solid angle	2.5%
μ Decay contamination	2 %
Efficiency	1.5%
Target absorption	1 %
Quadratic sum	4.2%

REFERENCES

1. S.D. Ecklund, R.L. Walker, Phys. Rev. 159, 1195 (1967).

2. H.A. Thiessen, Phys. Rev. 155, 1488 (1967).

3. G. Schwiderski, thesis, Karlsruhe (1967). G. Schwiderski and W. Schmidt, report 3/67-1, Kernforschungszentrum, Karlsruhe (1967).

4. Y.C. Chau, R.G. Moorhouse, N. Dombey, preprint, Glasgow University (1967).

5. E.A. Knapp, R.W. Kenney, V. Perez-Mendez, Phys. Rev. 114, 605 (1959).

6. M. Beneventano, R. Finzi, L. Mezzetti, L. Paoluzi, S. Tazzari, Nuovo Cimento, 28, 1464 (1963).

7. A.V. Tollestrup, J.C. Keck, R.M. Worlock, Phys. Rev. 99, 220 (1955).

8. M. Heinberg, W.M. Mc Clelland, F. Turkot, W.M. Woodward, R.R. Wilson, D.M. Zipoy, Phys. Rev. 110, 1211 (1958).

9. R.L. Walker, J.G. Teasdale, V.Z. Peterson, J.I. Vette, Phys. Rev. 99, 210 (1955).

10. J.C. Bizot, J. Perez-Y-Jorba, D. Treille, Proceedings of the Int. Symposium on Electron and Photon Interactions (Deutsche Physikalische Gesellschaft, Hamburg 1965) Vol. II.

11. R.A. Alvarez, Thick-Radiator Bremsstrahlung, HEPL 228 (1961) Stanford.

12. B. Milman, l'Onde Electrique 42, 310 (1962).

13. L.N. Hand, Phys. Rev. 129, 1834 (1963).

14. F.P. Dixon, R.L. Walker, Phys. Rev. Letters, 1, 458 (1958). Revised data in J.H. Boyden, Ph. D. Thesis, Cal. Inst. of Technology (1961).

15. D. Freytag, W.J. Schwille, R.J. Wedemeyer, Z. Physik 186, 1 (1965). C. Freitag, D. Freytag, K. Lübelsmeyer, W. Paul, Z. Physik, 175, 1 (1963).

16. K. Althoff, H. Fischer, W. Paul, Z. Physik, 175, 19 (1963).

17. A.J. Lazarus, W.K.H. Panofsky, F.R. Tangherlini, Phys. Rev. 113, 1330 (1959).

18. R.A. Alvarez, Phys. Rev. 142, 957 (1966).

19. L. Hand, C. Schaerf, Phys. Rev. Letters 6, 229 (1961).

20. C. Schaerf, Nuovo Cimento, 44, 504 (1966).

21. J. Engels, A. Müllensiefen and W. Schmidt, Contribution to the "Heidelberg International Conference on Elementary Particles" 1967 and to be published. See also W. Schmidt, Zeitschr. f. Physik 182, 76 (1964).

22. J. Engels and W. Schmidt, Phys. Rev. (to be published).

23. We use standard notations in pion photoproduction, see e.g. G.F. Chew, M.L. Goldenberger, F.E. Low, and Y. Nambu, Phys. Rev. 106, 1345 (1957) or ref. (21).

24. F.A. Behrends, A. Donnachie and D.L. Weaver, CERN report 67/146/5-TH.744, Geneva (1967).

25. A. Donnachie and G. Shaw, Ann. Phys. (N.Y.) 37, 333 (1966).

26. G.Buschhorn, J. Carroll, R.D. Eandi, P. Heide, R. Hübner, W. Kern, U. Kötz, P. Schmüser and H.J. Skronn, Phys. Rev. Letters 17 1027 (1966) and 18, 571 (1967).

27. J. Engels, W. Schmidt and G. Schwiderski, Phys. Rev. (to be published).

28. C. Lovelace, CERN report 65/1674/5-TH.628 (1965).

29. H.J. Lipkin, Phys. Letters 12, 154 (1964).

30. A. Donnachie, Phys. Letters 24B, 420 (1967).

31. A. Donnachie, R.G. Kirsopp and C. Lovelace, CERN report 67/1283/5-TH. 838, Geneva (1967).

FIGURE CAPTIONS

Fig. 1 Kinematics of the three experimental regions.

Fig. 2 Pion yield as a function of the electron energy (p and θ fixed).

Fig. 3 Experimental layout.

Fig. 4 Target setup.

Fig. 5 Optics of the triple focusing spectrometer (sketch).

Fig. 6 Optics of the mass spectrometer (sketch).

Fig. 7 Separation of positrons from pions with the mass spectrometer.

Fig. 8 Normalization process.

Fig. 9 Mean solid angle of the spectrometer as a function of momentum. (Note the vertical scale)

Fig. 10 Angular distribution in the c.m. system - The data points are as follows:

- ● This experiment.
- ▽ F.D. Dixon et al. (ref. 14).
- ▼ M. Heinberg et al (ref. 8).
- □ D. Freytag et al. (ref.15).
- ◐ M. Beneventano et al. (ref.6).
- ○ S.D. Ecklund et al. (ref.1,2).
- △ A.V. Tollestrup et al. (ref.7).
- ▲ R.L. Walker et al. (ref.9).
- ■ K. Althoff et al. (ref.16).
- ◇ L. Hand, C. Schaerf (ref.19,20).

Solid curve: ref.(21), dashed curve: ref.(3).

Fig. 11 Total cross sections (μb) as a function of the laboratory photon energy. Solid curve: ref.(21).

Fig. 12 Excitation curves (θ^* constant). Solid curve: ref.(21), dashed curve: ref. (3).

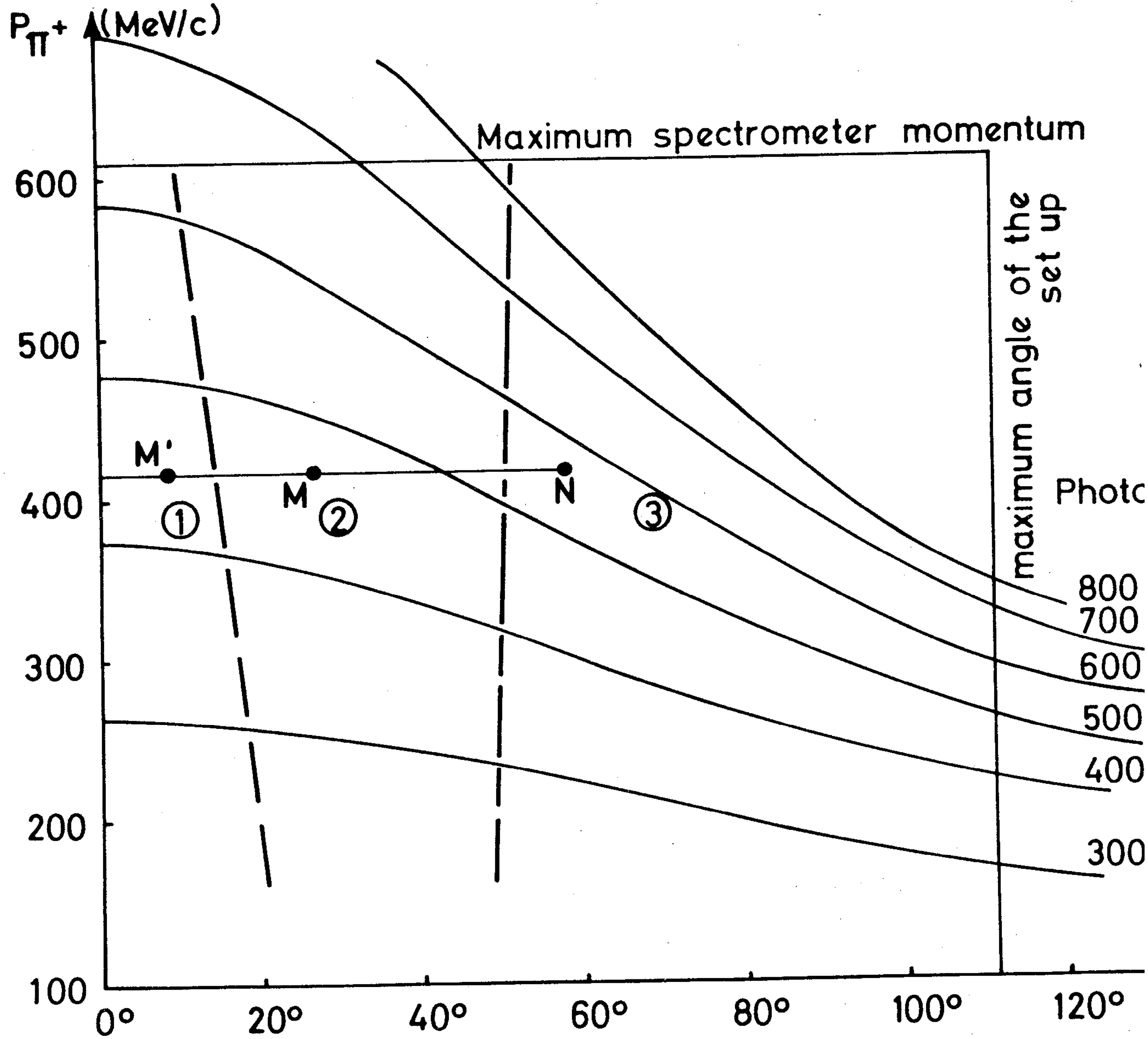

P_{π^+} (MeV/c)
Maximum spectrometer momentum
maximum angle of the set up
Photo
M'
M
N
1
2
3
800
700
600
500
400
300
600
500
400
300
200
100
0°
20°
40°
60°
80°
100°
120°

Fig. 1

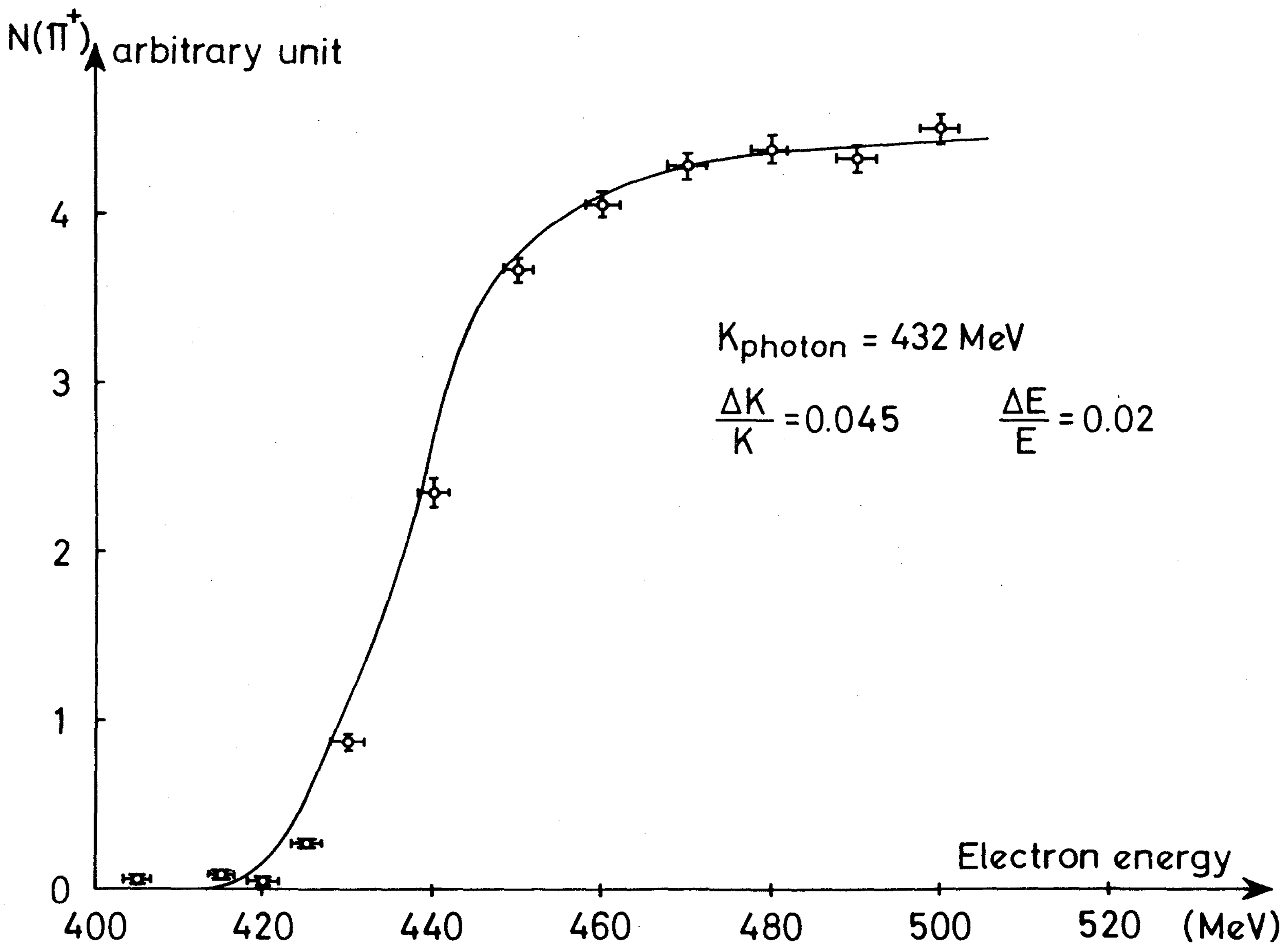
N(π⁺) arbitrary unit
4
3
2
1
0
K_{photon} = 432 MeV
$\frac{\Delta K}{K} = 0.045$
$\frac{\Delta E}{E} = 0.02$
Electron energy
400
420
440
460
480
500
520
(MeV)

Fig. 2

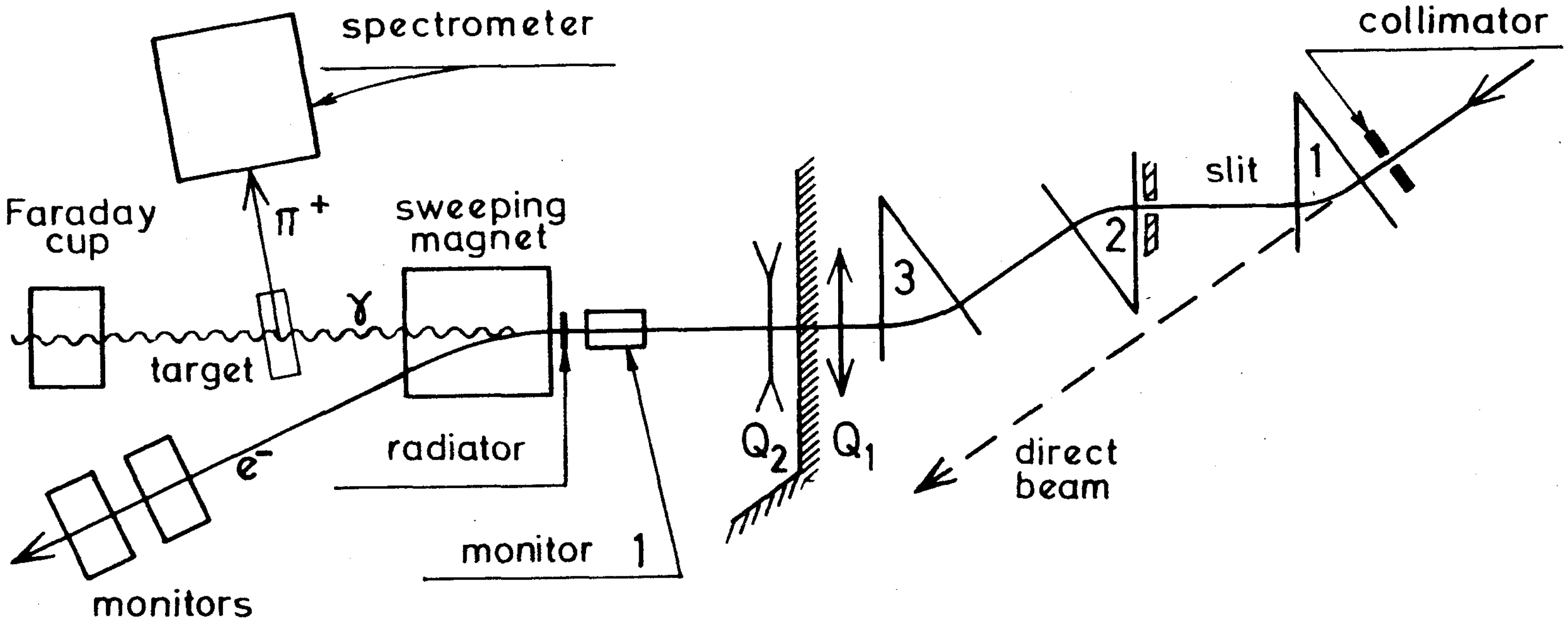
spectrometer
collimator
Faraday
cup
π^+
sweeping
magnet
γ
slit
1
2
3
target
radiator
Q_2
Q_1
direct
beam
e^-
monitor 1
monitors

Fig. 3

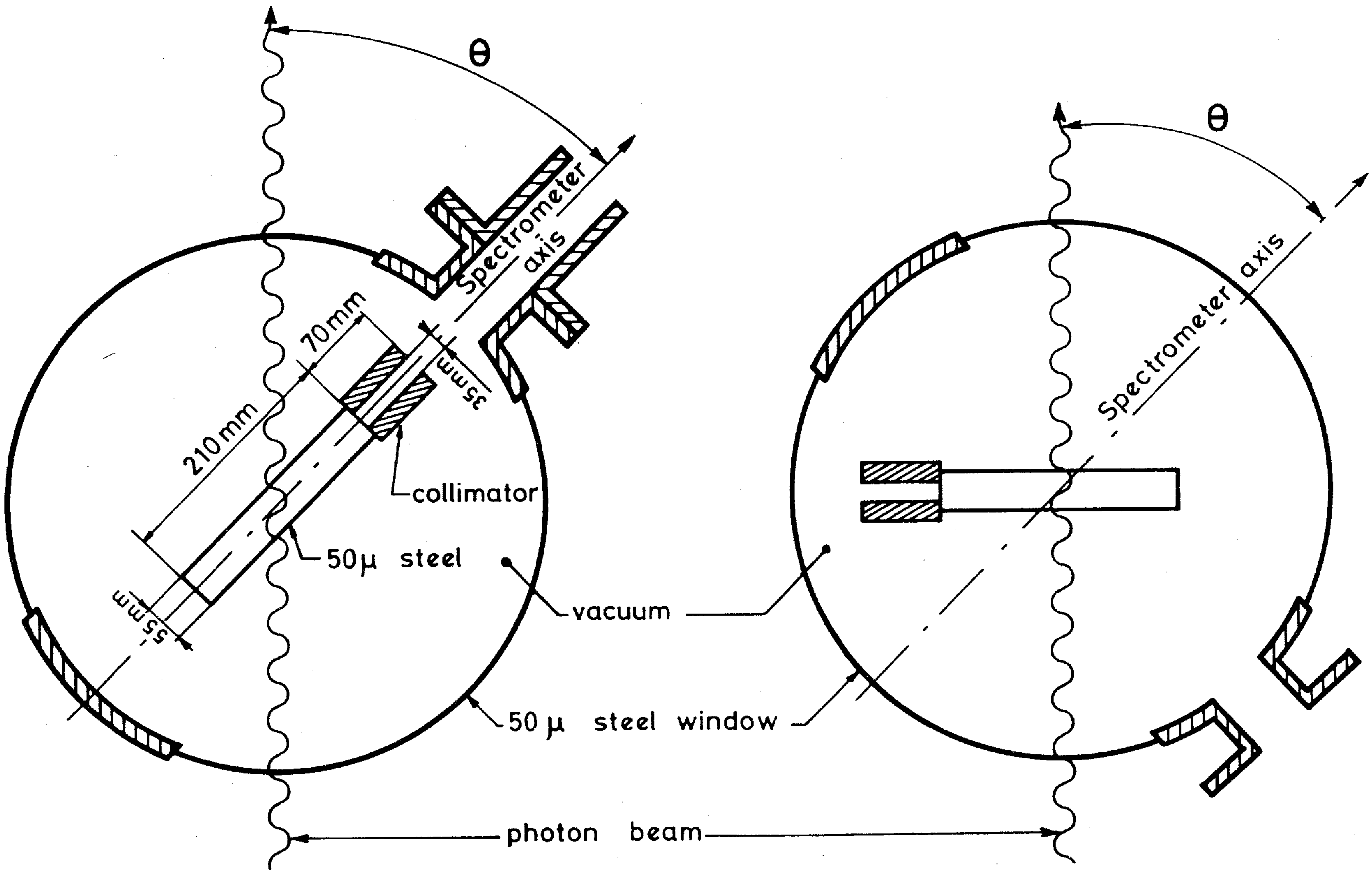
θ
Spectrometer axis
70mm
210mm
35mm
collimator
50μ steel
55mm
vacuum
50 μ steel window
photon beam
θ
Spectrometer axis

(4 - a)

(4 - b)

Fig. 4

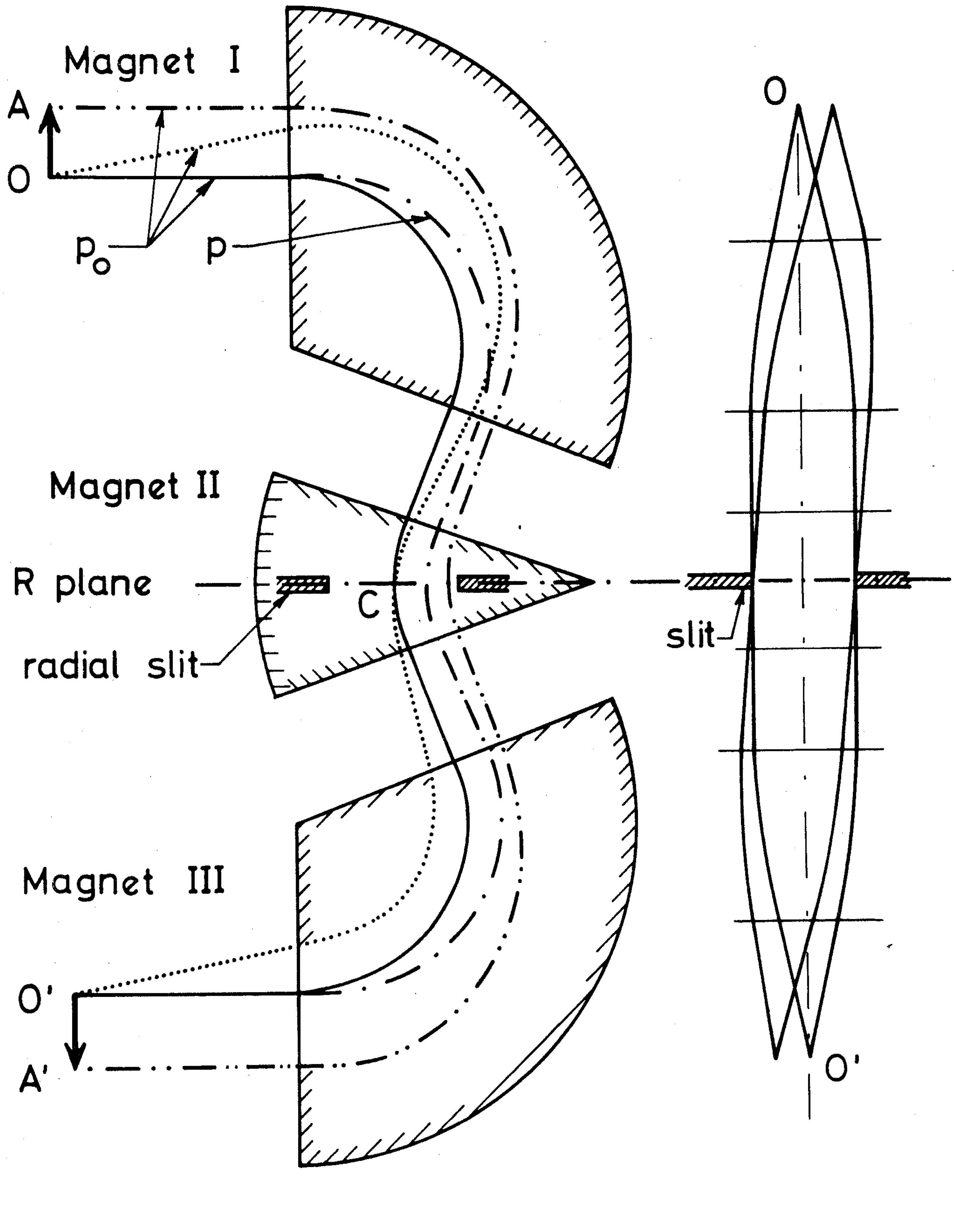

Magnet I
A
O
p_o
p
O
Magnet II
R plane
C
radial slit
slit
Magnet III
O'
A'
O'

Fig. 5

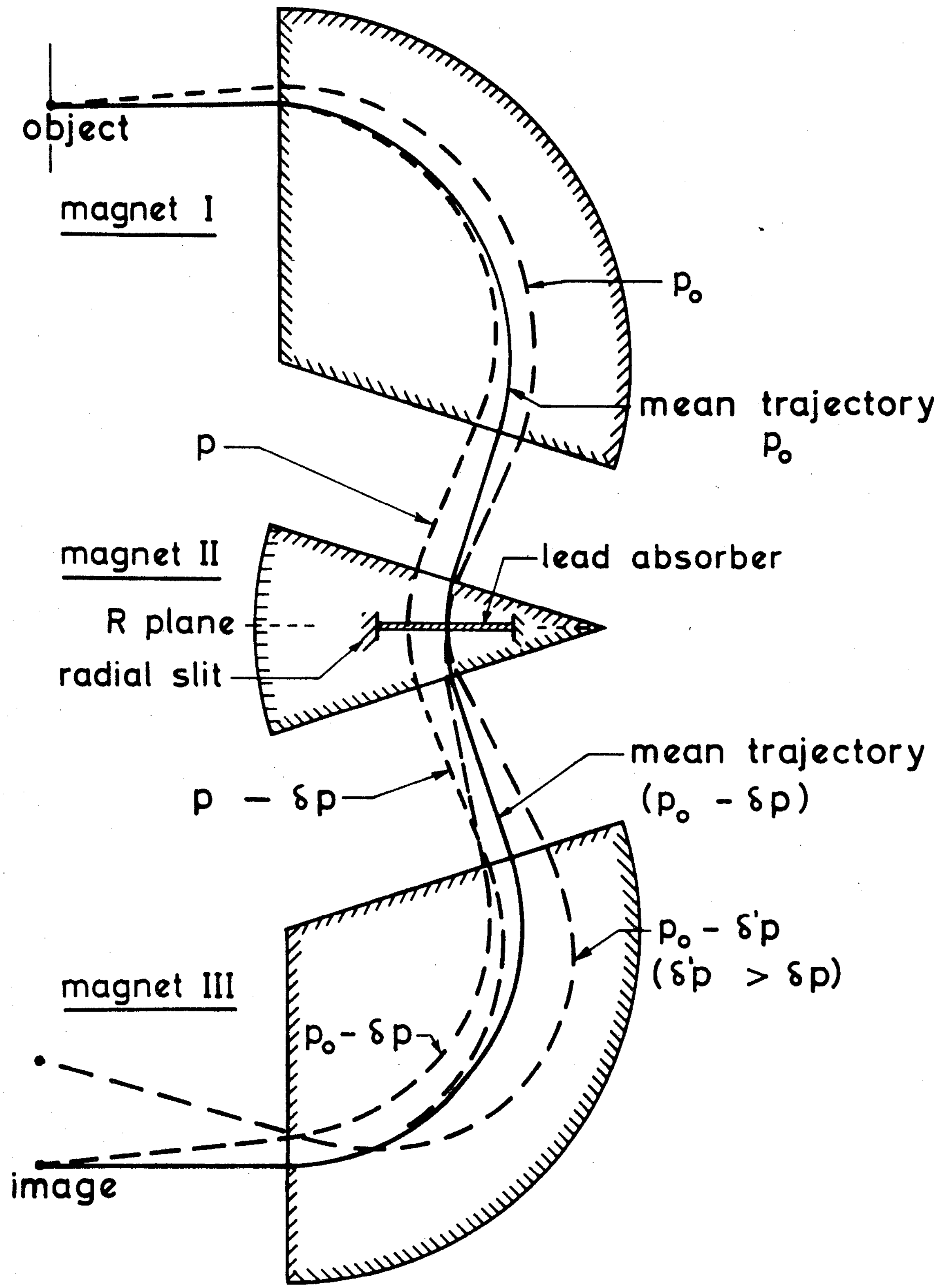
object
magnet I
p_o
mean trajectory
p_o
p
magnet II
lead absorber
R plane
radial slit
mean trajectory
$(p_o - \delta p)$
$p - \delta p$
$p_o - \delta' p$
$(\delta' p > \delta p)$
magnet III
$p_o - \delta p$
image

Fig. 6

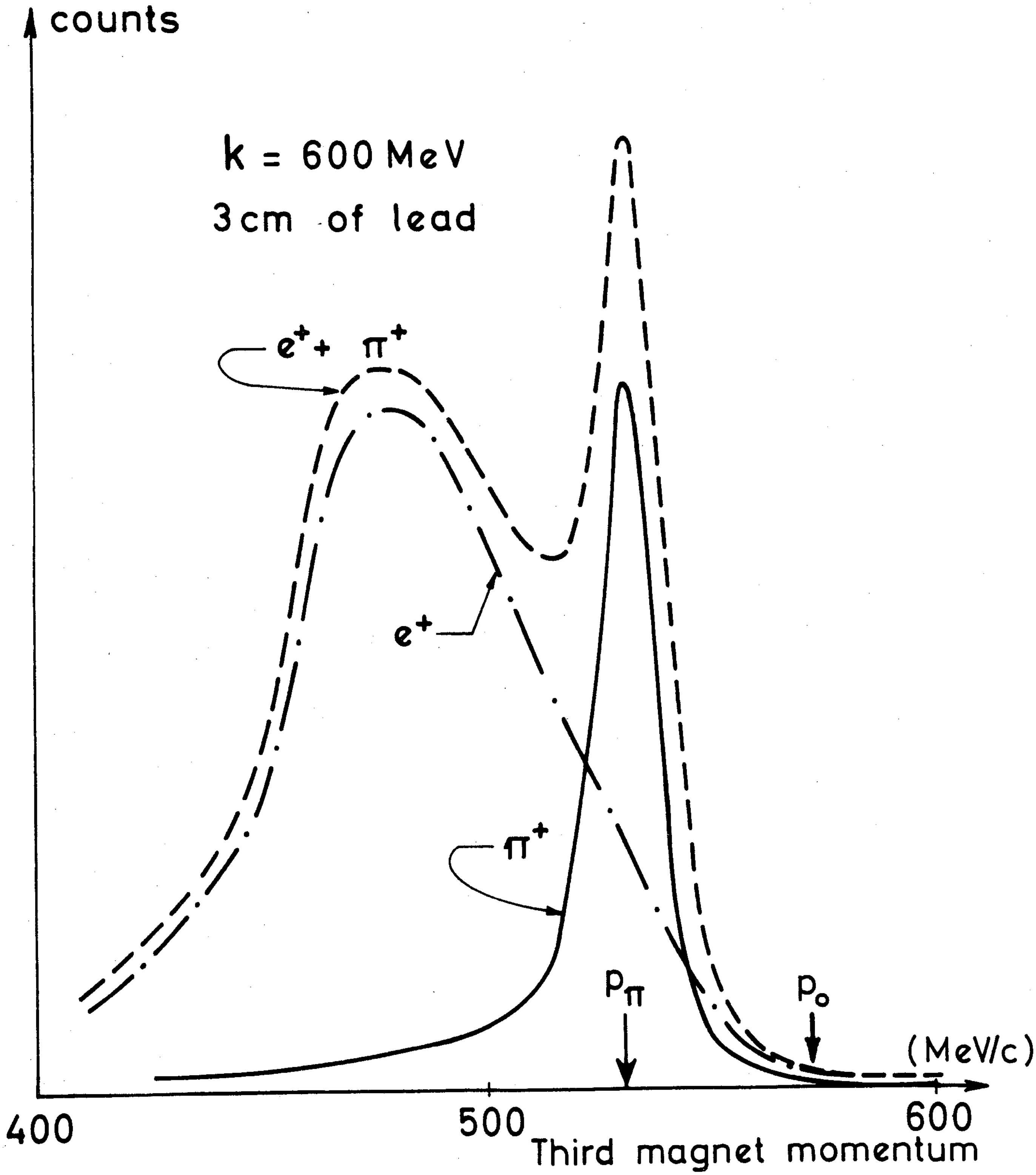
counts
k = 600 MeV
3 cm of lead
e⁺+ π⁺
e⁺
π⁺
p_π
p_o
(MeV/c)
400
500
600
Third magnet momentum

Fig. 7

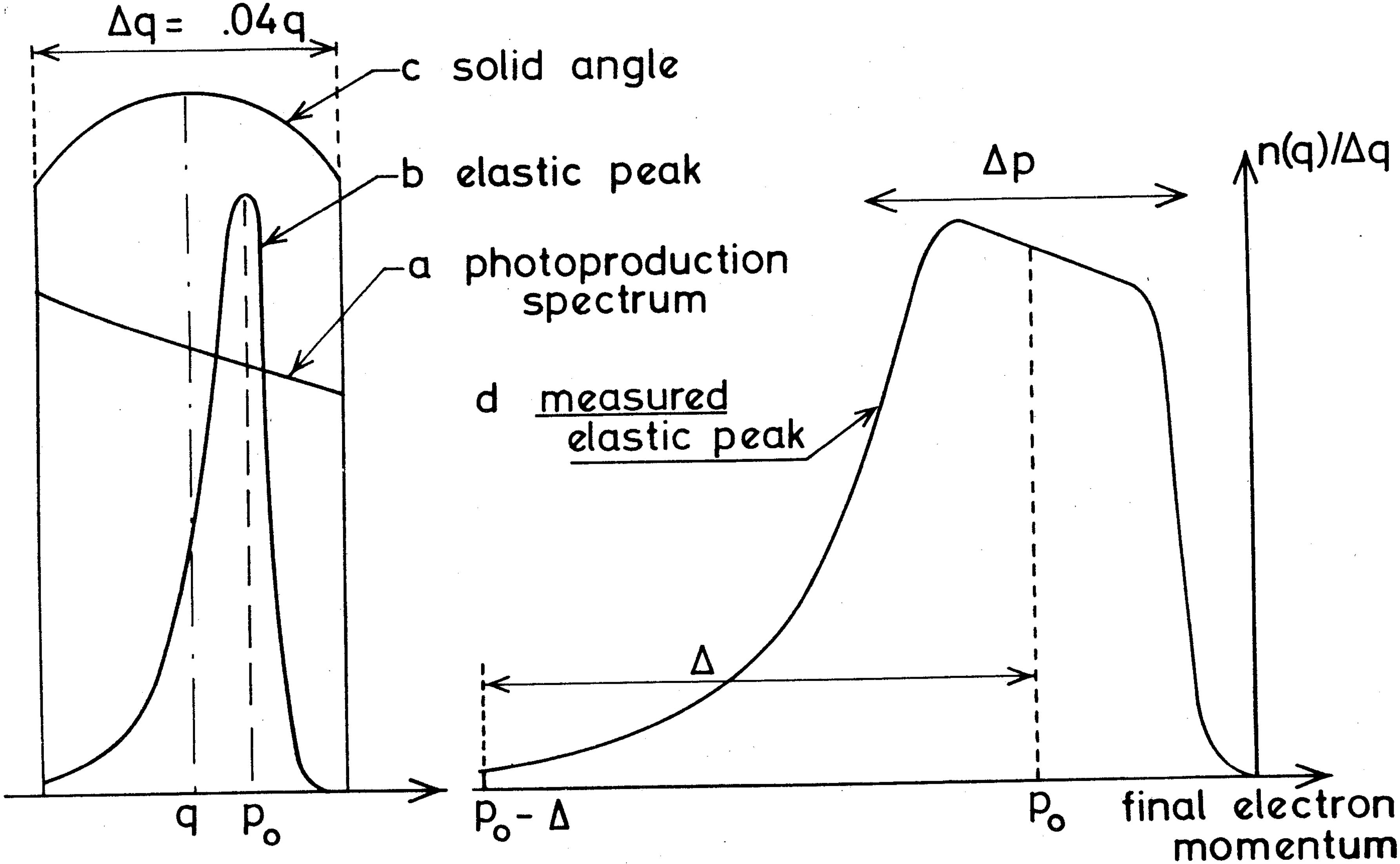

Δq = .04q
c solid angle
b elastic peak
a photoproduction
spectrum
q
p₀
Δp
n(q)/Δq
d measured
elastic peak
Δ
p₀ - Δ
p₀
final electron
momentum

Fig. 8

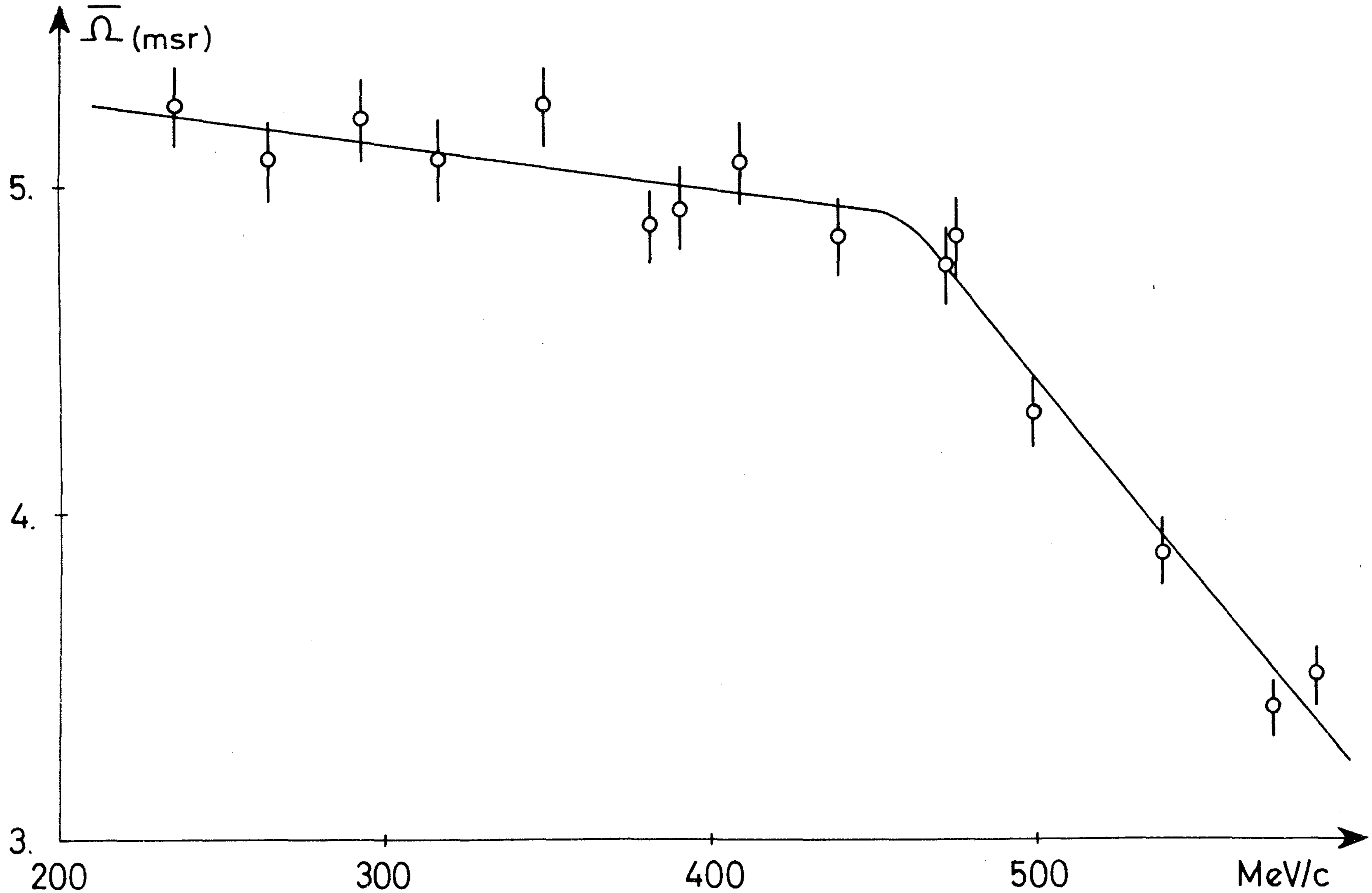

Fig. 9

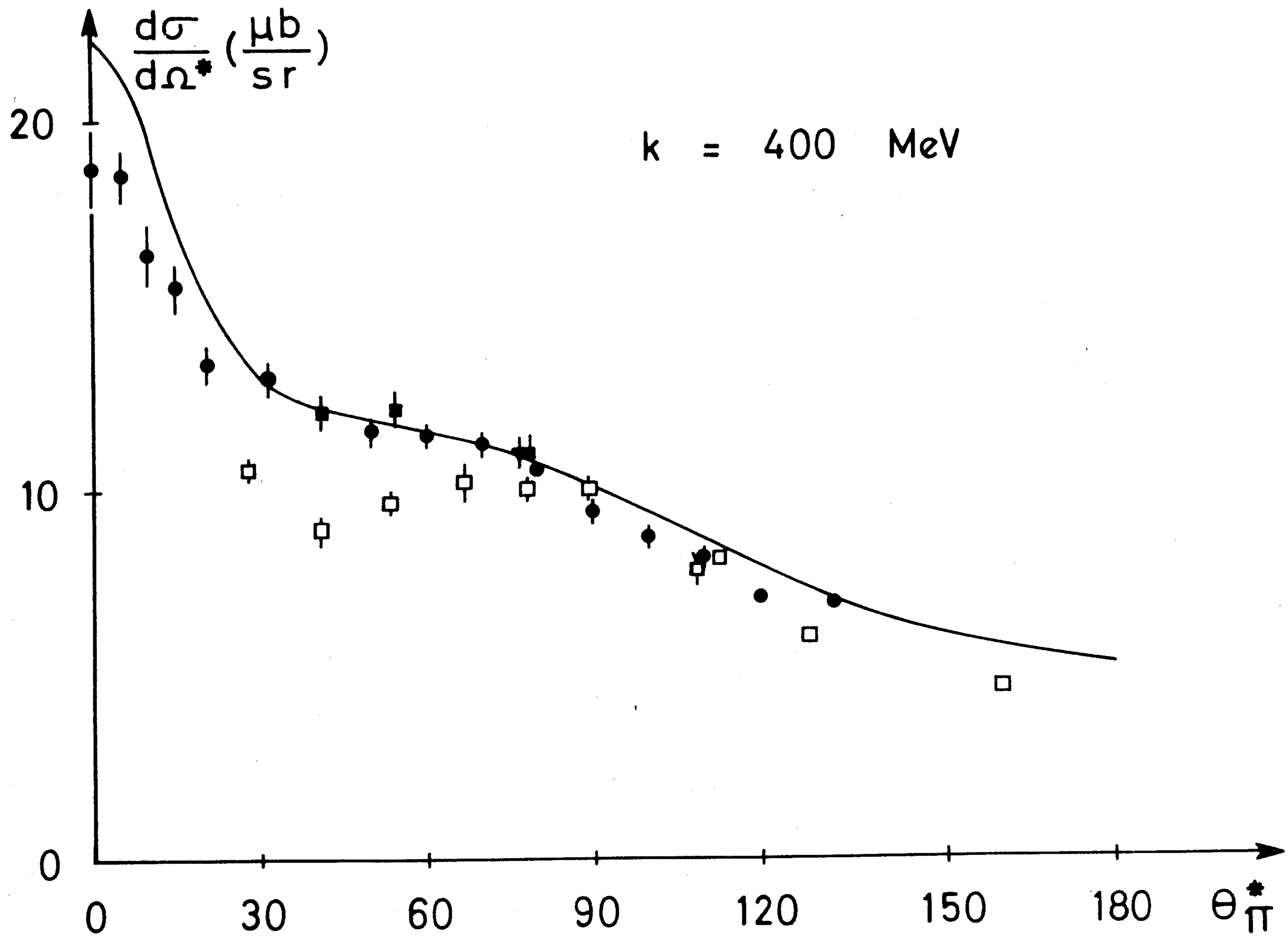
$\frac{d\sigma}{d\Omega^*}\left(\frac{\mu b}{sr}\right)$
k = 400 MeV
20
10
0
0
30
60
90
120
150
180
θ^*_π

Fig. 10

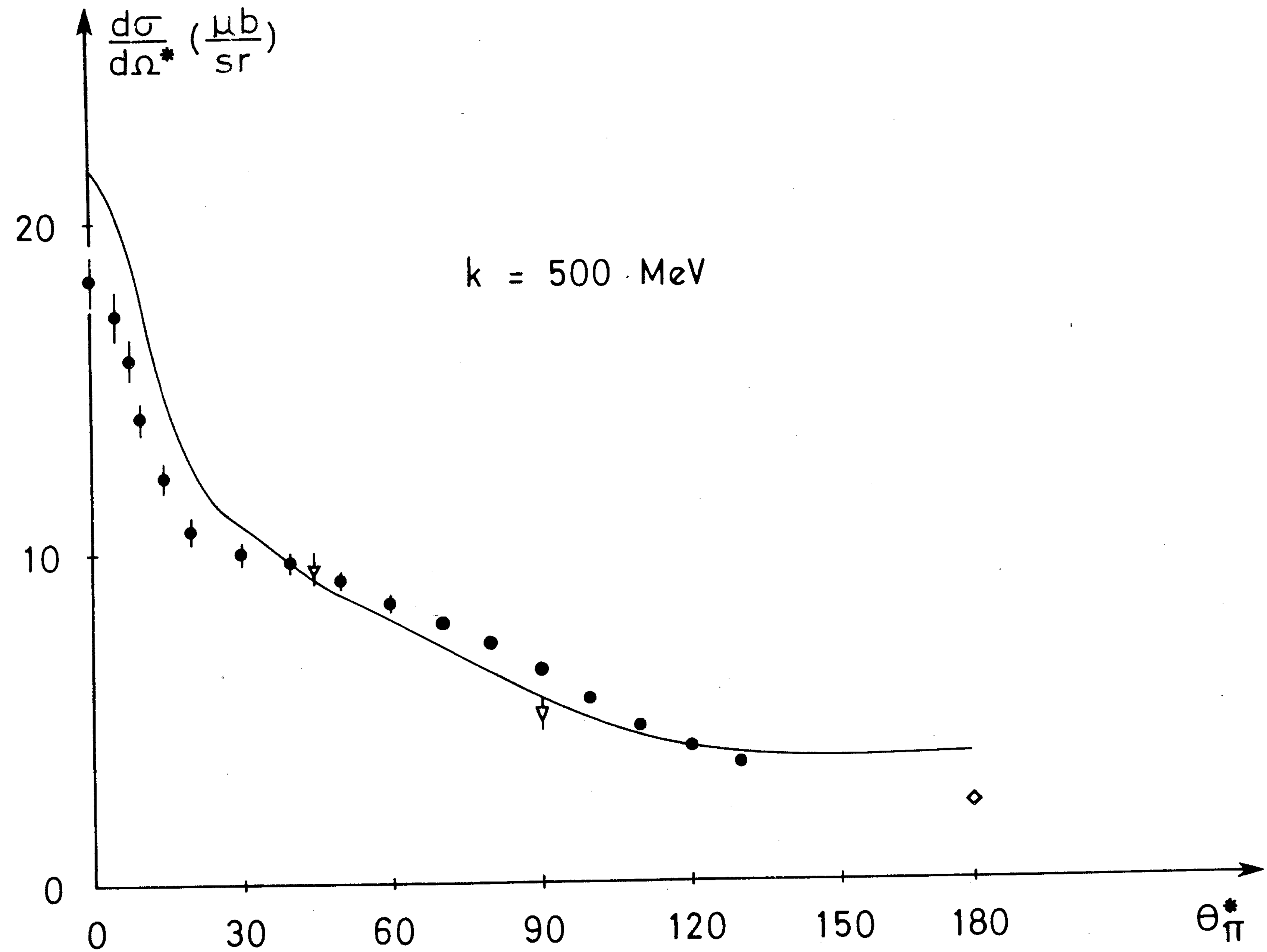

$\frac{d\sigma}{d\Omega^*}\left(\frac{\mu b}{sr}\right)$
20
10
0
k = 500 MeV
0
30
60
90
120
150
180
θ^*_π

Fig. 10

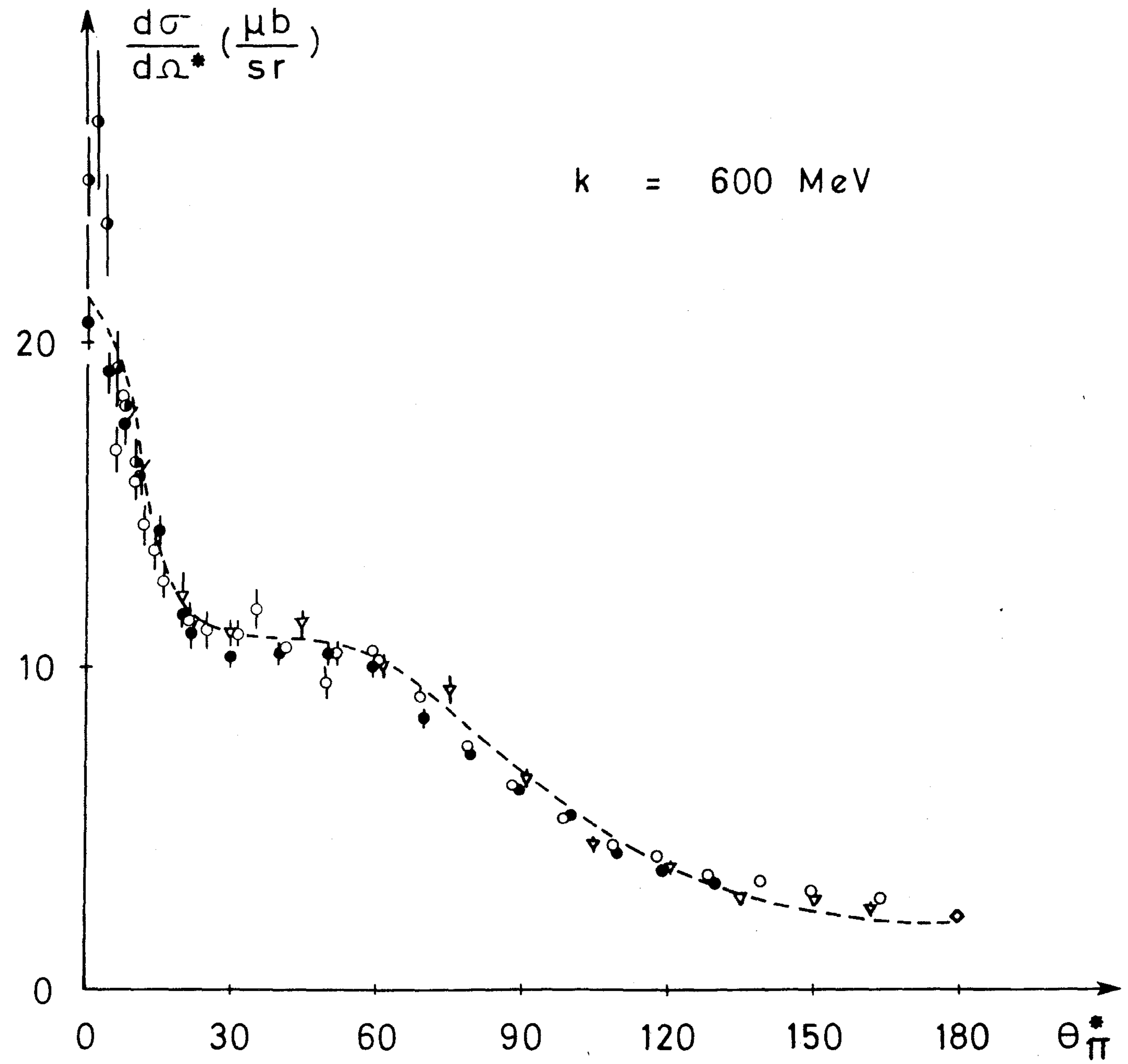
$\frac{d\sigma}{d\Omega^*}\left(\frac{\mu b}{sr}\right)$
k = 600 MeV
20
10
0
0
30
60
90
120
150
180
θ^*_π

Fig. 10

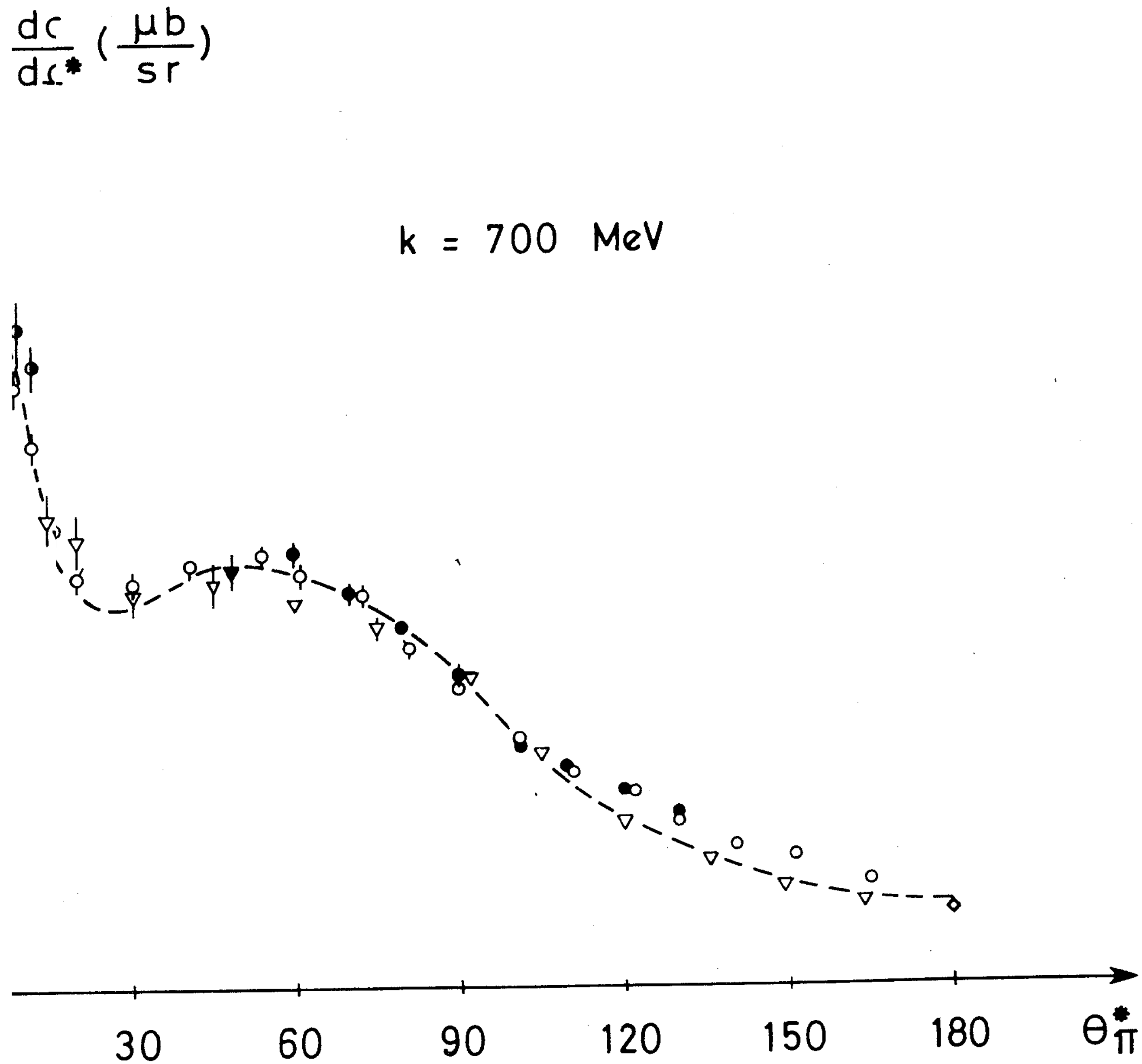

Fig. 10

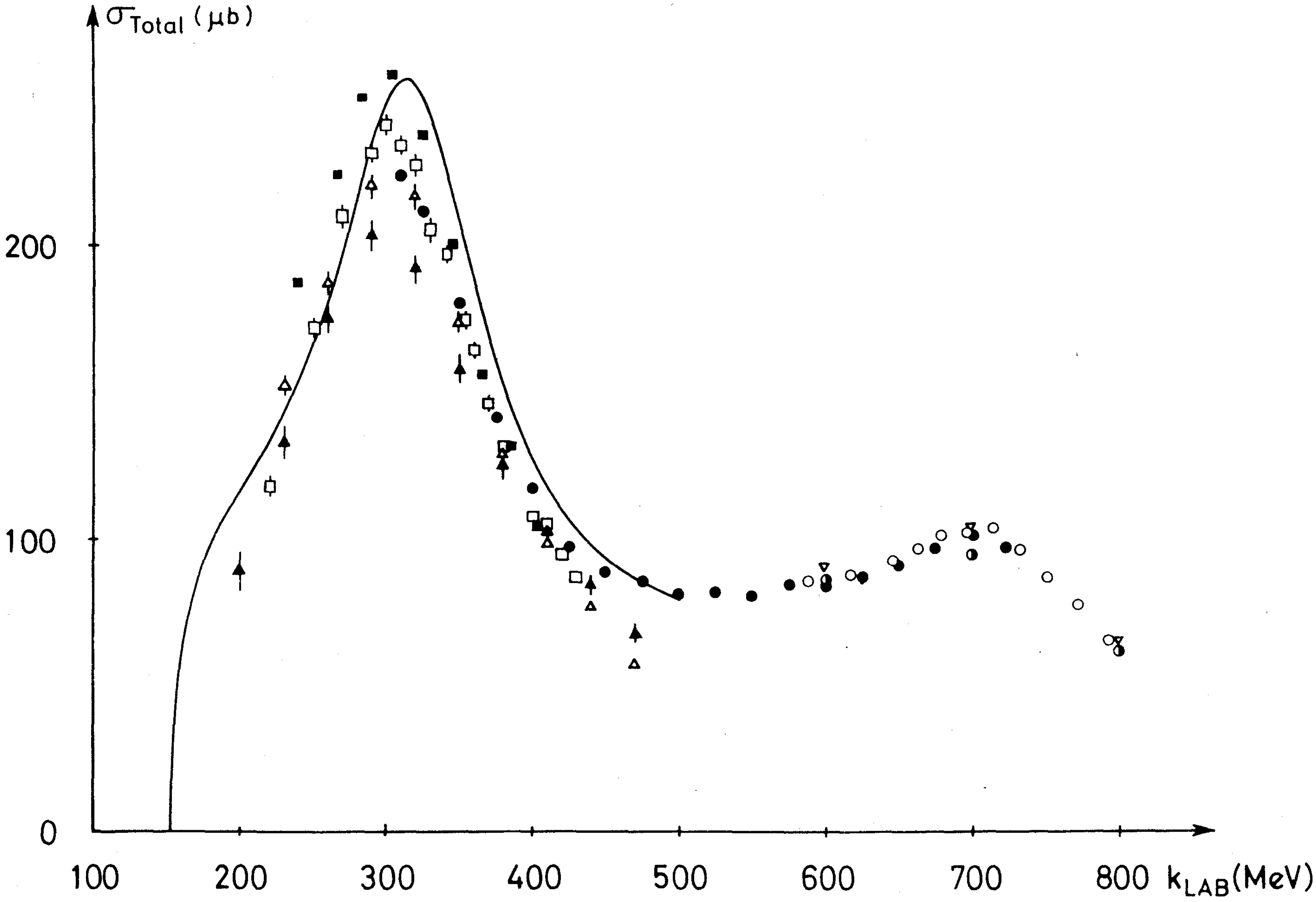

Fig. 11

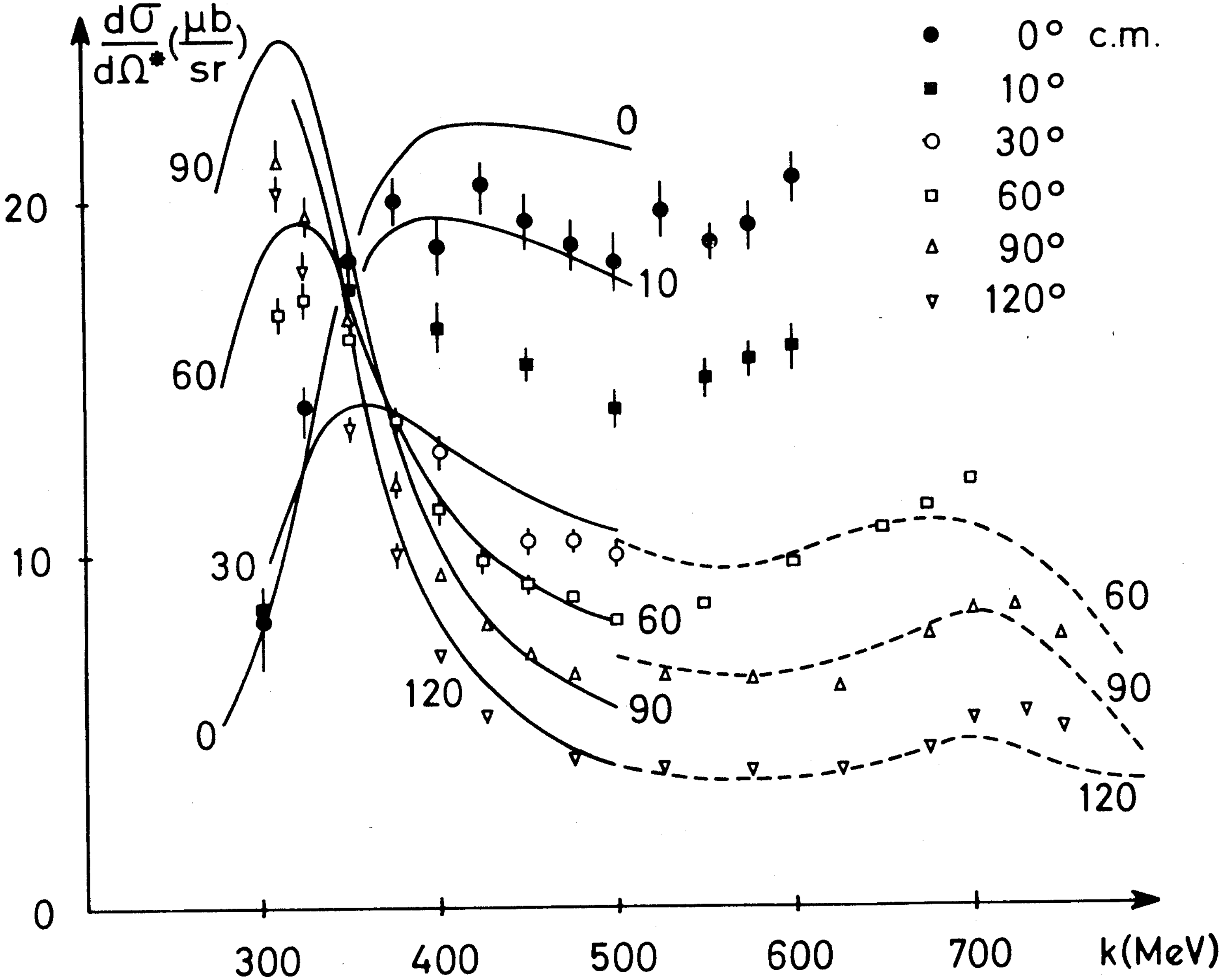

Fig. 12